JOURNAL OF SOLID STATE CHEMISTRY **127,** 283–294 (1996)
ARTICLE NO. 0385

Structural and Microstructural Studies of the Series $La_{2/3-x}Li_{3x}\square_{1/3-2x}TiO_3$

J. L. Fourquet, H. Duroy, and M. P. Crosnier-Lopez

Laboratoire des Fluorures, URA CNRS 449, Faculté des Sciences du Mans, Université du Maine, Avenue O. Messiaen, B.P. 535, 72017 Le Mans Cedex, France

Received February 29, 1996; in revised form September 23, 1996; accepted September 25, 1995

Much work has been done on the series $La_{2/3-x}Li_{3x}\square_{1/3-2x}TiO_3$ because of the high level of Li^+ ionic conductivity exhibited by this material. Curiously, the structural aspect was not yet really explored. We propose here a structural model for the series, in the composition range $0.06 < x < 0.14$, on the basis of X-ray powder diffraction and transmission electronic microscopy data: the symmetry is tetragonal (*P*4/*mmm*), and the unit cell derives from that of the perovskite ABO_3 ($a = a_p$, $c \sim 2a_p$). Vacancies, La, and Li ions are unequally distributed on two sites, 1*a* and 1*b*; the La distribution is approached by the Rietveld method from the X-ray powder patterns and confirmed by simulation of high resolution electron microscopy images.

INTRODUCTION

The field of the lithium ion-conducting materials has been widely studied because of their potential applications for solid electrolytes in high energy batteries and other electrochemical devices. One of the best lithium ion conductivities (greater than 10^{-4} S cm^{-1} at room temperature) was found by Inaguma *et al.* (1) and by Kawai and Kuwano (2) in the series $La_{2/3-x}Li_{3x}\square_{1/3-2x}TiO_3$.

If the ionic conductivity property is well established for this material, its crystal structure is not exactly known and is still under discussion. A simple cubic perovskite was first claimed for $La_{0.5}Li_{0.5}TiO_3$ (3) while other studies proposed an orthorhombic perovskite (4) or a tetragonal tungsten bronze structure (5, 6). Recently Varez *et al.* (7) studied the composition $La_{0.5}Li_{0.5}TiO_3$ and proposed a new tetragonal unit cell based on the cubic perovskite ($a = 2^{1/2}a_p$ and $c = 2a_p$) on the basis of X-ray diffraction and transmission electron microscopy studies.

This paper presents our structural results on the series $La_{2/3-x}Li_{3x}\square_{1/3-2x}TiO_3$ based on Rietveld treatment of the X-ray diffraction powder patterns and on transmission electron microscopy studies.

EXPERIMENTAL

The compositions corresponding to the series $La_{2/3-x}Li_{3x}\square_{1/3-2x}TiO_3$ were synthesized from stoichiometric amounts of La_2O_3, TiO_2, and Li_2CO_3 (high purity grade). The reagents were mixed and pressed into pellets and first heated in air for 4 h at 850°C in platinum boats. After regrinding and repressing, the samples were heated three times for 10 h at 1150°C and were allowed to cool in the furnace (naturally down to 200°C).

The chemical content (elemental weight %) was determined by the following methods. The samples were fused with potassium pyrosulfate and solved in N sulfuric acid. The lithium content was determined by flame photometry; results were Li% ± 0.05. Lanthanum content was determined by complexometric titration with EDTA 0.02 *N* and xylenol orange in a light acidic solution (pH 6 adjusted by hexamethylenetetramine); results were La% ± 1.50. Titanium content was determined by colorimetry (410 nm) of the yellow color produced by hydrogen peroxide with titanium(IV) in acidic solution; results were Ti% ± 0.4. Owing to the good agreement found within the limits of accuracy between analytical and nominal values, it was decided to retain the later for the sample chemical composition.

The samples were characterized by X-ray powder diffraction on a D500 Siemens diffractometer (T = 20°C; radiation Cu$K\alpha$; 2θ range, 9°–129°; step $\Delta 2\theta$, 0.04°; time by step, 18 s) and the patterns were analyzed through the Rietveld method by the FULLPROF program (8).

The TEM study (electron diffraction and high resolution) was performed with a JEOL 2010 electron microscope operating at 200 kV and equipped with a side-entry ±30° double tilt specimen holder. High-resolution multislice simulations were carried out with the EMS programs of Stadelman (9) using the following microscope parameters:

0022-4596/96 $18.00

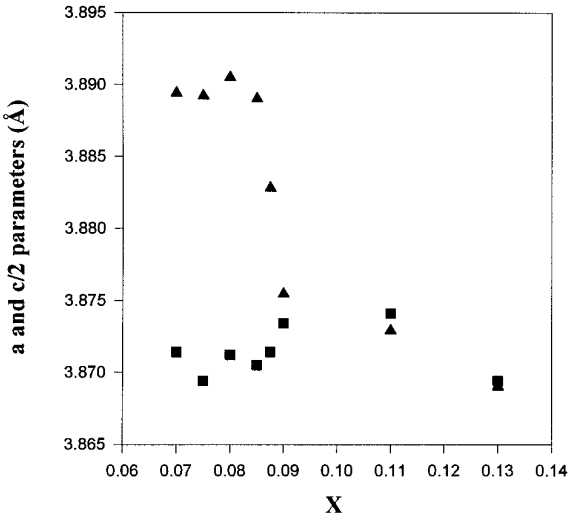

FIG. 1. Evolution of the unit cell parameters versus x (a, squares; $c/2$, triangles).

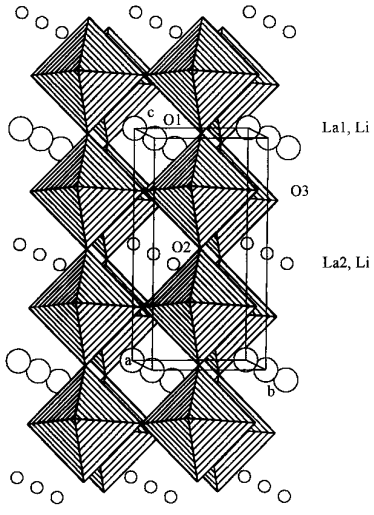

FIG. 2. Structural model ($P4/mmm$).

—acceleration voltage, 200 kV;
—spherical aberration constant, Cs = 1.0 nm;
—defocus spread, Δ = 12 nm;
—semi-convergence angle, α = 0.8 mrad;
—objective lens aperture diameter, 11.6 nm^{-1}.

TEM specimen preparation was carried out by dispersing ultrasonically small particles in *n*-butanol and disposing drops of this suspension on a Cu grid covered with a holey carbon film.

EDX analysis was performed on numerous crystals, with a KEVEX energy dispersive X-ray spectrometer coupled with the TEM. La, Ti, and O were always found together in the samples but it was not possible to do quantitative analysis of different terms of the solid solution taking account of the small variations of La: for $x = 0.06$, $\%_{La}$ = 12.7 and for $x = 0.14$, $\%_{La} = 10.7$ (at. %).

RESULTS AND DISCUSSION

(*a*) *X-Ray Powder Analysis*

For the series $La_{2/3-x}Li_{3x}\square_{1/3-2x}TiO_3$, a pure phase was found in the domain $0.06 < x < 0.14$, a result in good agreement with the study of Kawai and Kuwano (2). Many other compositions were unsuccessfully examined around this line in the ternary system La_2O_3–Li_2O–TiO_2 in order to check the existence of a more extended solid solution domain.

TABLE 1
$La_{2/3-x}Li_{3x}\square_{1/3-2x}TiO_3$: Structural Model in the Space Group *P4/mmm*

Atom	Position	Atomic coordinates (x, y, z)
La1 + Li + □	1*a*	0, 0, 0
La2 + Li + □	1*b*	0, 0, 1/2
Ti	2*h*	1/2, 1/2, $z \approx 0.25$
O1	1*c*	1/2, 1/2, 0
O2	1*d*	1/2, 1/2, 1/2
O3	4*i*	0, 1/2, $z \approx 0.25$

At room temperature, all the patterns were easily indexed in a primitive tetragonal cell deriving from that of the cubic perovskite ABO_3 ($a = a_p \approx 3.87$ Å and $c \approx 2a_p$) and with a $c/2a$ distortion decreasing for high lithium content. This evolution rules out, from our point of view, the interpretation of Robertson *et al.* (10) who claimed the existence of two different tetragonal unit cells, characterized by different $c/2a$ distortion values. It is also to be noticed that we did not find any line leading to a double cell like that proposed by Varez *et al.* (7). The width and the intensity of the diffraction lines, which impose the doubling of the c axis, vary with the composition: these superstructure lines (with $l = 2n + 1$) become less intense and broader as the lithium content grows. These facts are, respectively, related to changes in the A sites population and to a more and more disordered structure along the c axis as discussed below. Figure 1 shows the evolution of the lattice parameters versus the composition. We observe that the tetragonal distortion $c/2a$ vanishes strongly near $x = 0.08$. These results are in agreement with those of Kawai and Kuwano (2).

This kind of superstructure was already found in $La_{2/3}TiO_{3-\delta}$ (11) with A-site deficient perovskite structure; in this compound, it is assumed that La and vacancies are ordered in the cages of the perovskite network. In order to approach the crystal structure of the material $La_{2/3-x}Li_{3x}\square_{1/3-2x}TiO_3$, we propose the simple model in the space group $P4/mmm$ reported in Table 1 and shown in Fig. 2. It is characterized by a distribution of vacancies

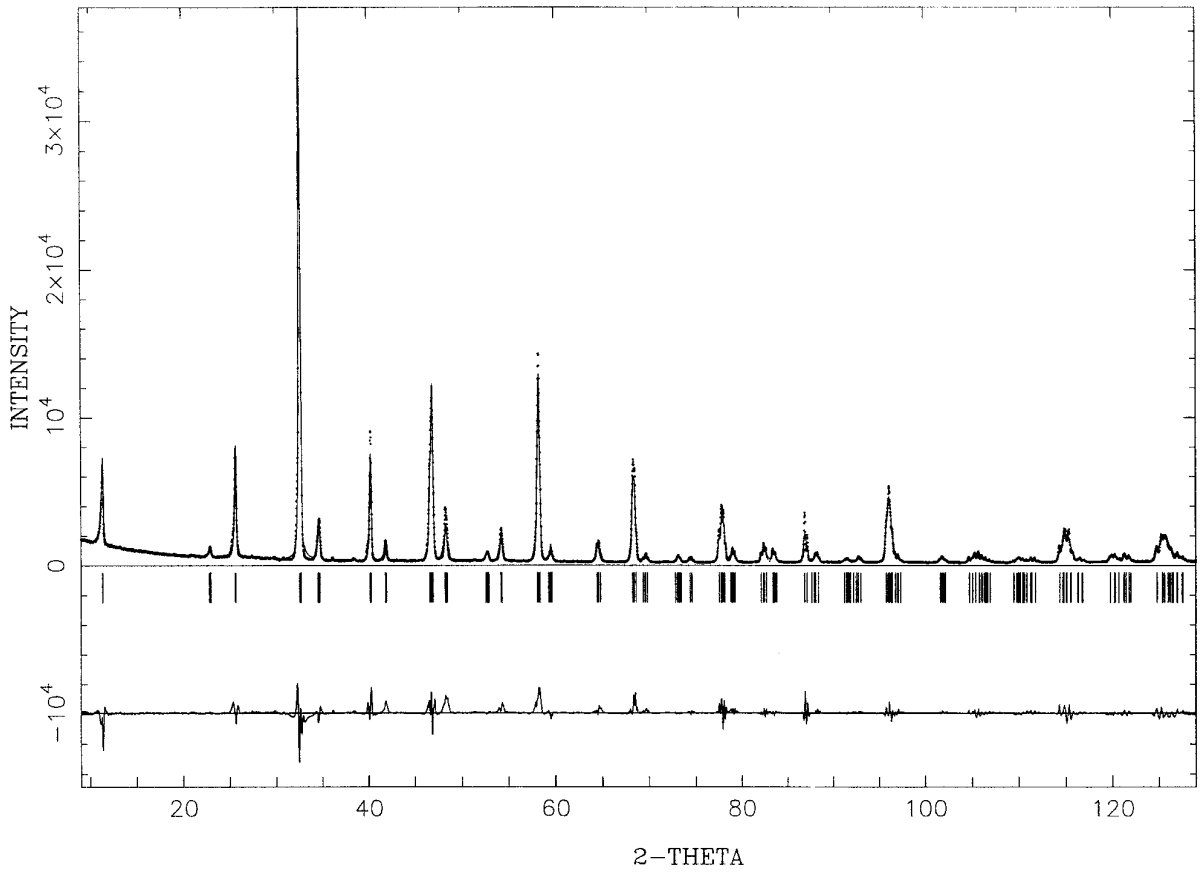

FIG. 3. Calculated and observed (...) X-ray diffraction patterns for $x = 0.07$. The difference spectrum is below at the same scale.

and of La and Li cations on the two sites 1*a* and 1*b*; we call La1 and La2 the La^{3+} ions located in the 1*a* and 1*b* positions, respectively. In a practical way, owing to the poor value of the Li^+ scattering factor, we decide to omit its contribution and to allow the La^{3+} content to be refined between 1*a* and 1*b* sites. In order to overcome the problem of the broadening of the superstructure lines (with $l = 2n + 1$) in the composition range $0.075 < x < 0.14$, we use for the pattern adjustment the two phases option of the FULLPROF program: with this method the two "phases," defined by the two sets of *hkl* lines corresponding, respectively, to $l = 2n$ and $l = 2n + 1$, present the same structural model and differ only by their linewidth parameters. For example, Figs. 3 and 4 present the good agreement obtained between the observed and calculated patterns for $x = 0.07$ (one "phase") and $x = 0.11$ (two "phases"). Table 2 presents the crystallographic characteristics for the two compositions. The broadening of the superstructure lines is related to the presence of antiphase domains (12); this phenomenon creates a disordered situation in the regular succession ... La1–La2–La1 ... along the *c* axis. An annealing at 600°C for 10 days for the compo-

TABLE 2
$La_{2/3-x}Li_{3x}\square_{1/3-2x}TiO_3$: Crystallographic Characteristics for $x = 0.07$ and 0.11 (in italic)

	Number of atoms	*x*	*y*	*z*	*B* (Å^2)[a]
La1	0.88, *0.784*	0	0	0	−0.33(2), *−0.20(2)*
La2	0.304, *0.32*	0	0	1/2	−0.33(2), *−0.20(2)*
Ti	2	1/2	1/2	0.2678(4) *0.2670(6)*	−0.33(4), *−0.32(4)*
O1	1	12	1/2	0	1.36(9), *1.39(7)*
O2	1	1/2	1/2	1/2	1.36(9), *1.39(7)*
O3	4	0	1/2	0.2538(8) *0.251(1)*	1.36(9), *1.39(7)*

Note. For $x = 0.07$, 174 intensities, 17 parameters, $R_I = 11.3$, $R_p = 20.7$, $R_{wp} = 24.1$, $a = 3.8714(1)$, $c = 7.7789(3)$ Å. For $x = 0.11$, "Phase 1," 82 intensities (*hkl* with $l = 2n + 1$), $R_I = 16.8$; "Phase 2," 92 intensities (*hkl* with $l = 2n$), $R_I = 7.42$; 22 parameters, $R_p = 17.1$, $R_{wp} = 16.6$, $a = 3.8741(1)$, $c = 7.7459(5)$ Å.

[a] B factors are kept, respectively, at the same values for La1 and La2 and for all the O atoms.

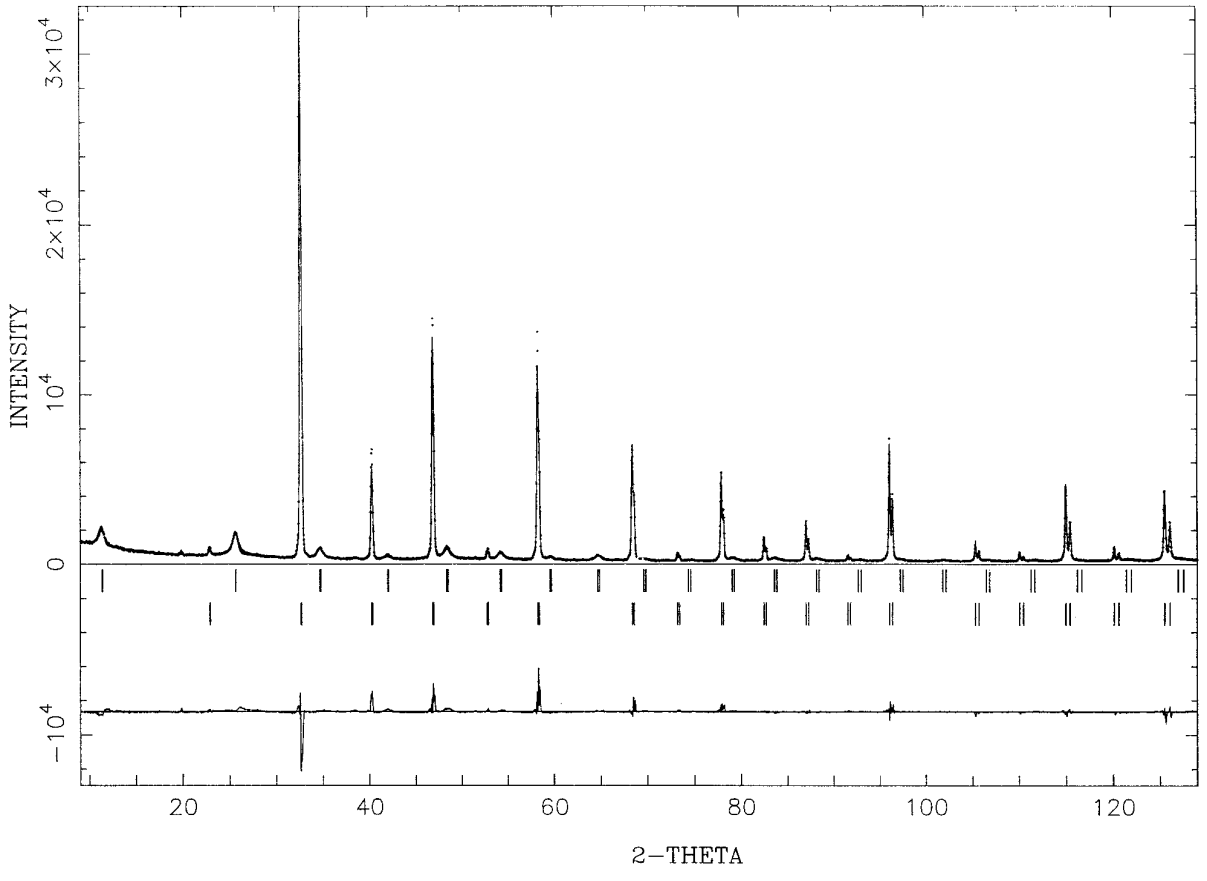

FIG. 4. Calculated and observed (...) X-ray diffraction patterns for $x = 0.11$. The difference spectrum is below at the same scale. The small line at $2\theta \approx 20°$ is the strong line of the $Li_2Ti_3O_7$ pattern.

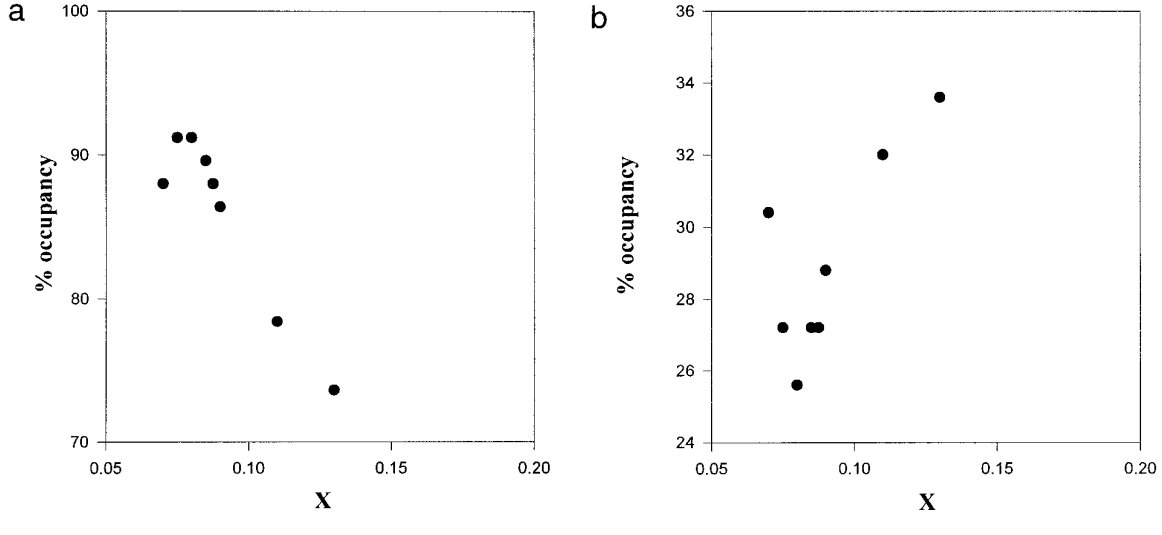

FIG. 5. La occupancy rates versus composition (a) for site 1*a* (0, 0, 0), La1; (b) for site 1*b* (0, 0, 1/2), La2.

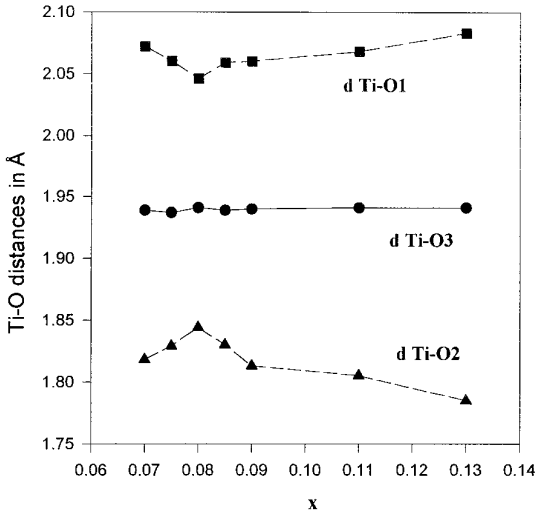

FIG. 6. Evolution of the Ti–O interatomic distances versus composition.

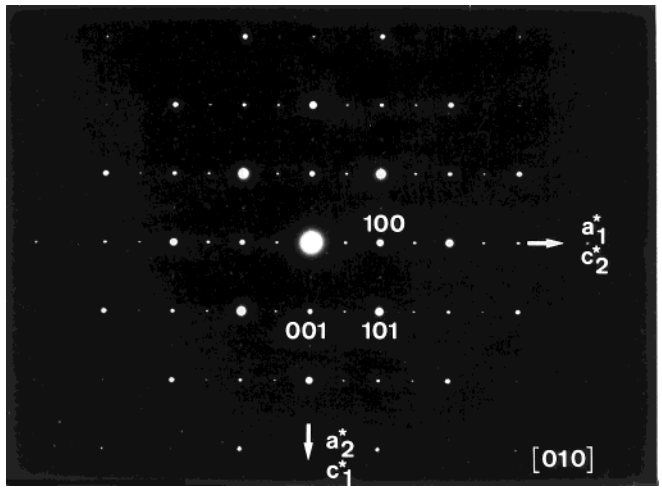

FIG. 7. Typical selected area diffraction pattern for all x values of the solid solution: ⟨100⟩ zone axis. Miller indices correspond to spots of an 'ideal' cubic ($a = a_p$) perovskite cell.

sition $x = 0.11$ was without any effect on the width of the superstructure diffraction lines.

Figure 5 presents the evolution of the La distribution over the two sites 1*a* (0, 0, 0) and 1*b* (0, 0, 1/2) with the composition. It can be seen that site 1*a* is markedly preferred by La^{3+} and that the introduction of Li^+ increases the cationic disorder on the *A* sites. The maximum La occupancy rate for site 1*a* is observed for an x value near 0.08, corresponding to the composition exhibiting the maximum tetragonal distortion of the unit cell (Fig. 1).

Our model does not take into account the Li^+ ions and the vacancies. We suppose of course that they both partly occupy the two sites 1*a* and 1*b*, the global formulation being $La_{2/3-x}Li_{3x}\square_{1/3-2x}TiO_3$.

The TiO_6 octahedra are distorted along the *c* axis with one short Ti–O2 distance (≈1.8 Å) opposed to one long Ti–O1 distance (≈2.0 Å) and four equal Ti–O3 distances (≈1.94 Å). The mean Ti–O distance, 1.94 Å, remains very stable for all the compositions studied; it is a value very close to the sum of the ionic radii, 1.955 Å, for Ti^{4+} and O^{2-} (13). The preferential location of the La^{3+} ions in the 1*a* site probably causes the displacement of Ti^{4+} toward the O2 atom; this is also the case in $La_{0.33}NbO_3$ (14) where Nb atoms are displaced along the *c* axis toward the layer of empty cuboctahedra. It is interesting to see (Fig. 6) that the Ti–O3 distance remains very stable whatever the composition while Ti–O1 and Ti–O2 distances vary in opposite sense (Table 3).

The La1 and La2 ions (in 1*a* and 1*b* sites, respectively) are 12-fold coordinated (4 O1 + 8 O3 for La1, and 4 O2 + 8 O3 for La2) in the very slightly distorted cuboctahedral cages of the perovskite structure. Table 3 gathers the La–O distances in both cases; their mean value, 2.74 Å, is in good agreement with the sum of the ionic radii for La^{3+} and O^{2-}, 2.71 Å (13). It is interesting to notice that this distance is on the contrary very large if we take into account the fact that these cages contain also Li^+ ions with a much smaller ionic radius than La^{3+}; this steric factor strongly favors here the Li^+ ionic mobility.

TABLE 3
$La_{2/3-x}Li_{3x}\square_{1/3-2x}TiO_3$: Selected Interatomic Distances in Å

x	dTi–O1	dTi–O2	4 × dTi–O3	4 × dLa1–O1	8 × dLa1–O3	4 × La2–O2	8 × La2–O3
0.07	2.072(3)	1.818(3)	1.939(4)	2.738(5)	2.75(4)	2.74(5)	2.74(5)
0.075	2.060(3)	1.829(3)	1.937(4)	2.736(4)	2.76(3)	2.736(4)	2.73(4)
0.08	2.046(2)	1.844(2)	1.941(3)	2.74(5)	2.71(2)	2.74(5)	2.77(2)
0.085	2.059(4)	1.830(4)	1.939(5)	2.74(5)	2.74(6)	2.74(5)	2.74(6)
0.09	2.060(3)	1.813(3)	1.940(3)	2.74(3)	2.74(1)	2.74(3)	2.74(3)
0.11	2.068(5)	1.805(5)	1.941(5)	2.74(5)	2.75(6)	2.74(5)	2.73(6)
0.13	2.083(5)	1.785(5)	1.941(7)	2.74(1)	2.73(3)	2.74(5)	2.74(6)

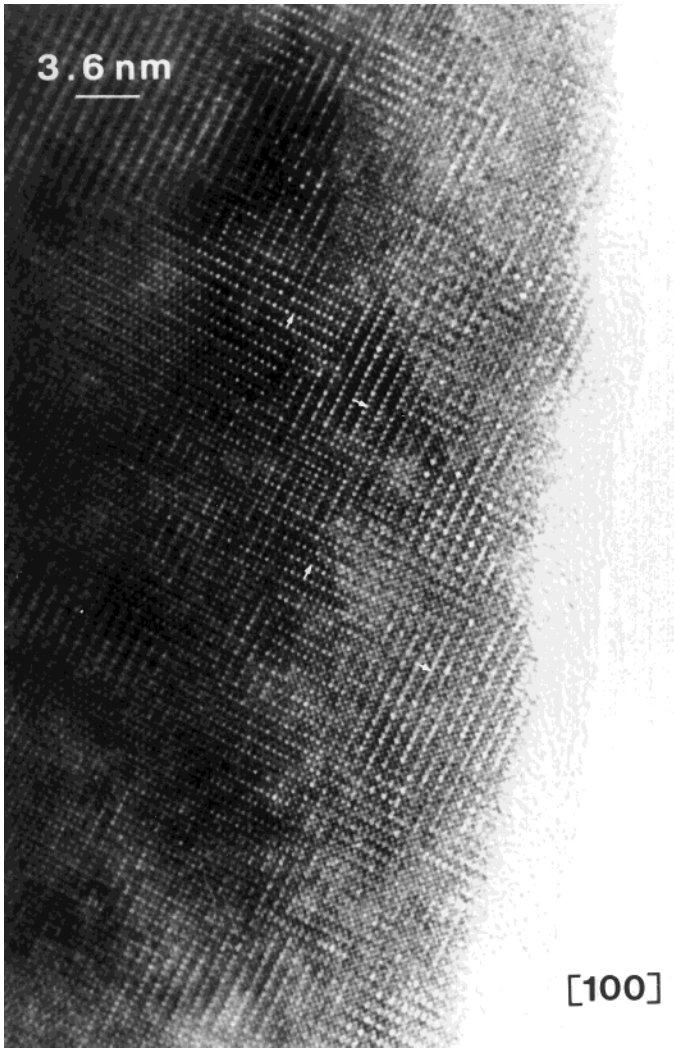

FIG. 8. ⟨100⟩ HREM image for a multiwinned typical crystal from the composition x = 0.11 showing a mosaic structure with small 90° oriented domains which give a SAED pattern such as Fig. 7 (white arrows mark [001] directions).

(*b*) *Electron Diffraction Study*

The electron diffraction study was performed on several crystals arising from different compositions and the reconstitution of their reciprocal space from ED patterns led always to an apparent cubic cell with the parameter $a \approx 2a_p$.

A typical ED pattern observed is shown in Fig. 7 and can be indexed with a cubic perovskite cell ($\langle 100 \rangle_p$ zone axis). The corresponding HREM image (Fig. 8) exhibits a more complex situation with a "patchwork contrast": a mosaic structure is formed by a lot of small domains (maximum size close to one hundred Å^2 for $x = 0.11$). Larger monodomains are impossible to observe and selected area diffraction patterns are always "twinned" due to the very small size of the domains. Meanwhile, for $x = 0.08$ (the maximum of tetragonal distortion of the unit cell), the domains are often elongated, some hundred Å^2 to almost one thousand Å^2 (Fig. 9). However, they are rarely large enough to observe untwinned patterns even if the smallest selected area aperture is used.

Optical diffraction experiments, carried out on different domains for a crystal of the composition $x = 0.08$, propose either the cell $a_p \times a_p$ or the cell $a_p \times 2a_p$ (Fig. 10), confirming thus the unit cell deduced from the X-ray powder analysis. Finally, it must be noted that such oriented domains can be formed easier when the ratio $c/2a$ is close to 1 (e.g., for $x = 0.11$). Under such conditions, the ED pattern observed in Fig. 7 can be explained by the superposition of three ED patterns of different domains in which the *c* axis is randomly oriented along the three space directions. If this result agrees with our powder study, it is in complete disagreement with the study of A. Varez *et al.* (7) who propose a diagonal supercell, $\sqrt{2}a_p \times \sqrt{2}a_p \times 2a_p$, leading to a cell volume twice ours which seems unnecessary to describe this solid solution.

FIG. 9. ⟨100⟩ low resolution image for a typical crystal from the composition $x = 0.08$ showing larger 90° oriented domains which give a SAED pattern such as Fig. 7 (white arrows mark [001] directions).

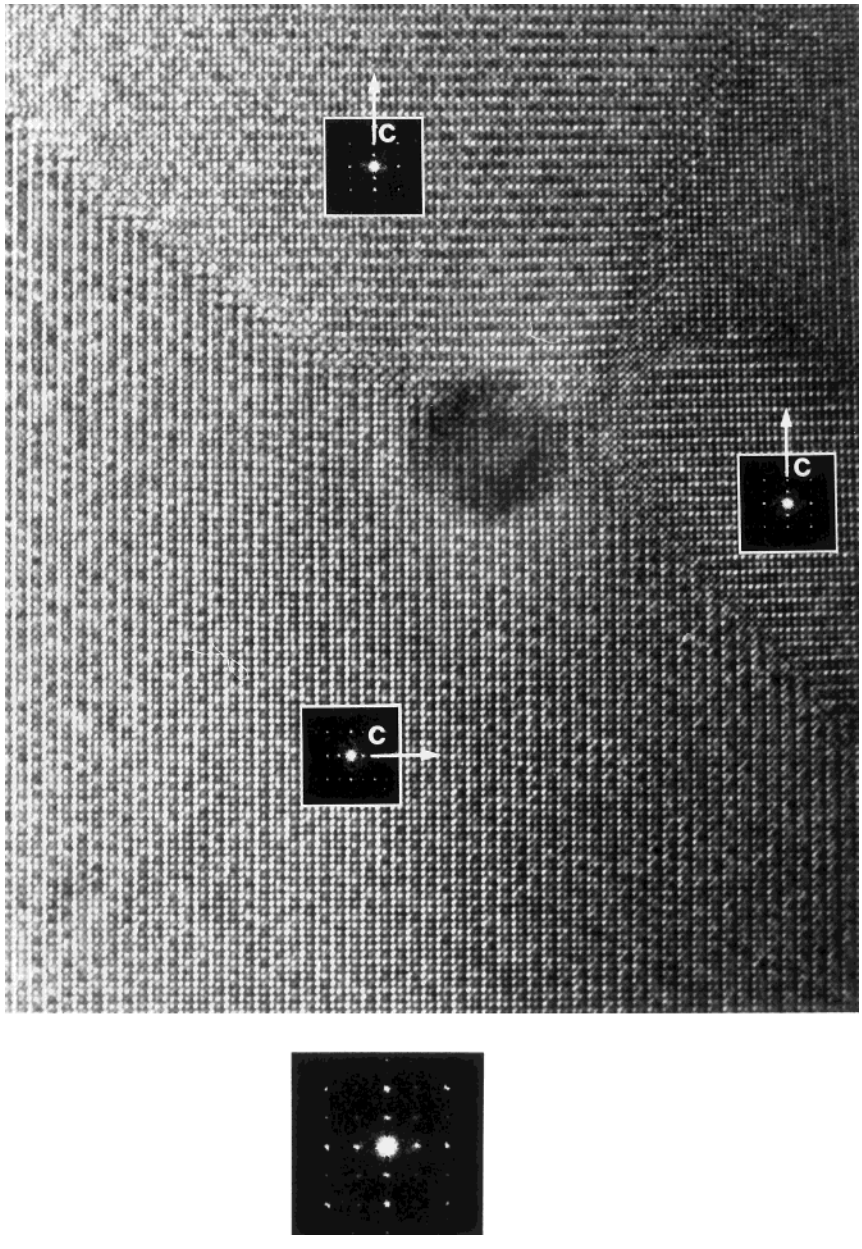

FIG. 10. Optical diffraction pattern of several domains 90° oriented showing two possible orientations of the *c* axis and in the lower part of the figure, the resultant optical diffraction pattern ($x = 0.08$).

Such a patchwork contrast has already been observed in related perovskites (15–18) as in superconducting copper oxides (19).

In Fig. 8, small domains (20–60 Å) are statistically distributed to form a tweed pattern with boundaries aligned either parallel to $(100)_p$ and $(010)_p$ or to $(110)_p$ and $(1\bar{1}0)_p$. Whereas, in Fig. 9, the boundaries of the larger elongated domains are predominantly parallel to $(110)_p$ and $(1\bar{1}0)_p$. An example of a coherent interface between two domains with a boundary parallel to $[110]_p$ is shown in Fig. 11 for a crystal taken in a sample $x = 0.08$.

As mentioned by A. Varez (7), some weak cross shaped diffuse spots can be often seen (Fig. 12) at $(1/2\ 1/2\ 0)_p$ and related positions: their arms are parallel to $[100]_p$ and $[010]_p$. M. Labeau *et al.* (17–20) have realized structural studies on different $ThNb_4O_{12}$ samples, an *A*-cation-deficient perovskite-related phase. They have shown that the origin of these crosses can be due to the microdomain structure (the orientation of the diffuse crosses are directly related to those of the domain boundaries) but also to an *A*/vacancy ordering (preferential localization of cations along some directions). In our case, these two phenomena

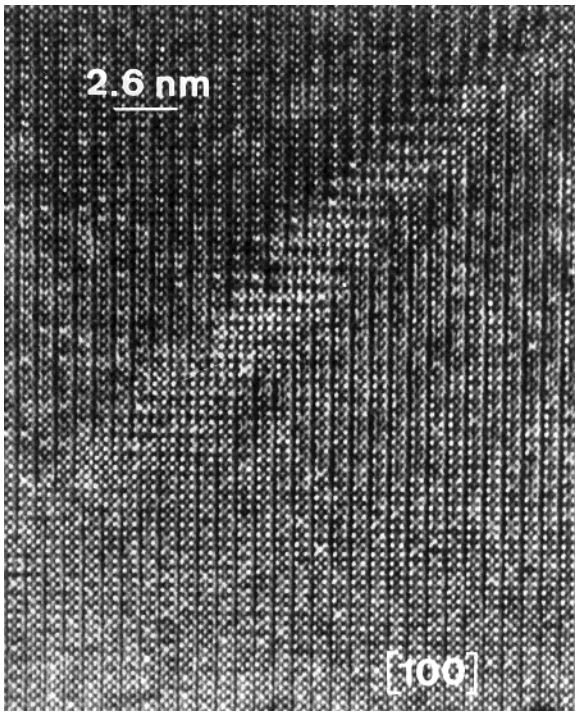

FIG. 11. ⟨100⟩ HREM image of a crystal ($x = 0.08$) exhibiting a coherent interface between the domains.

can be both responsible for the observed situation. Nevertheless, such crosses are not always observed on different crystals examined for the same preparation and do not allow us to be conclusive on these phenomena.

(*c*) ⟨*100*⟩ *HREM Imaging*

Taking into account the size of the domains, the HREM study was performed on the sample $x = 0.08$, which was assumed to be homogeneous. All the simulated images of this work have been calculated by the multislice method with the results proposed by the X-ray diffraction powder study: space group *P*4/*mmm* (No. 123), cell parameters, and atomic coordinates of the atoms (excepted Li atoms) are from the Table 4. For $x = 0.08$, the total number of La atoms is 1.168, with a preferential occupation of site 1*a*: 91.2% for La1 (site 1*a*) and 25.6% for La2 (site 1*b*).

TABLE 4
$La_{2/3-x}Li_{3x}\square_{1/3-2x}TiO_3$: Crystallographic Characteristics for $x = 0.08$

Space group *P*4/*mmm*
$a = 3.87$ Å
$c = 7.78$ Å

	Number of atoms	*x*	*y*	*z*
La1	0.912	0	0	0
La2	0.256	0	0	1/2
Ti	2	1/2	1/2	0.2630
O1	1	1/2	1/2	0
O2	1	1/2	1/2	1/2
O3	4	0	1/2	0.2446

The ⟨100⟩ projection of the structure seems to be a good orientation to test the sensitivity of the HREM image contrast to the La occupancy since the columns of cations La1 and La2 are separated (Fig. 13). In this structure projection, three different types of cationic rows perpendicular to the *c* direction can be distinguished. The first type of rows consists in only Ti atoms (B) along the *b* axis, the second is built up only with La atoms on the 1*a* site (A), and the third is built up only with La atoms on the 1*b* site (C). Two successive rows are regularly spaced of $a_p/2$. The stacking sequence along the *c* axis is then ABCB.

With this object, we have simulated images for different La1 and La2 occupancy rates with a total number of La atoms equal to 1.168. Figure 14 displays simulated

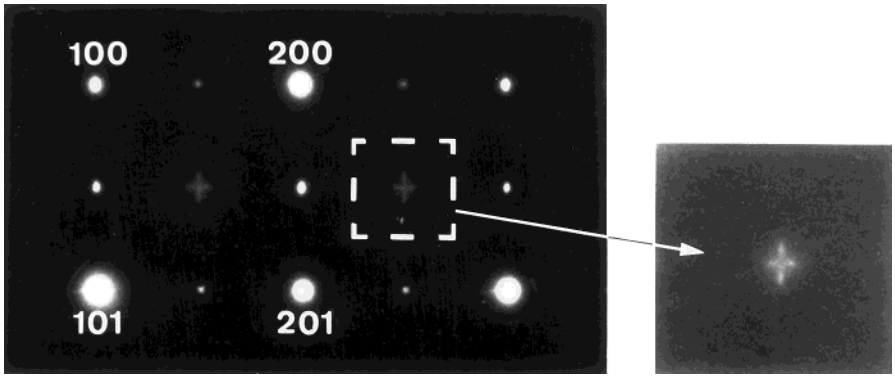

FIG. 12. Enlargement of a selected area diffraction pattern along ⟨100⟩ showing diffuse crosses which arms are parallel to $[100]_p$ and $[001]_p$. Miller indices correspond to spots of an 'ideal' cubic ($a = a_p$) perovskite cell ($x = 0.11$).

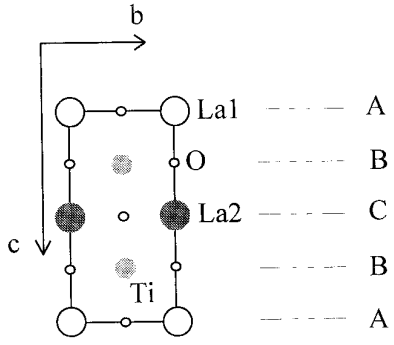

FIG. 13. ⟨100⟩ projection of the structure showing the three types of rows A, B, and C and their stacking sequence along the *c* axis.

images (slice thickness 0.1936 nm, sampling 128 × 64, specimen thickness 2.3 nm, defocus range $-40 \leq \Delta f \leq -100$ nm) for three different La1 and La2 occupancy rates:

Site 1*a*	100%	80%	60%
Site 1*b*	16.8%	36.8%	56.8%
Figure	14a	14b	14c

(The last distribution corresponds nearly to a statistical distribution of the La on the two sites 1*a* and 1*b*).

At a thickness of 2.3 nm, a La1 site with an occupancy rate close to 60% means that for this column containing six cation positions, two or three vacancies (or Li cations) may be detected. Under our imaging conditions, the comparison between the simulated HREM images allow us to remark that the contrast is more sensitive to the respective population of the two sites for defocus values in the range from −40 to −60 nm. However, it seems really more difficult to estimate exactly their respective population, taking into account the contrast evolution in function of the La population. In the case of statistical distribution of La cations over their respective sites (c case), the typical contrast of the perovskite-type oxides should be observed for defo-

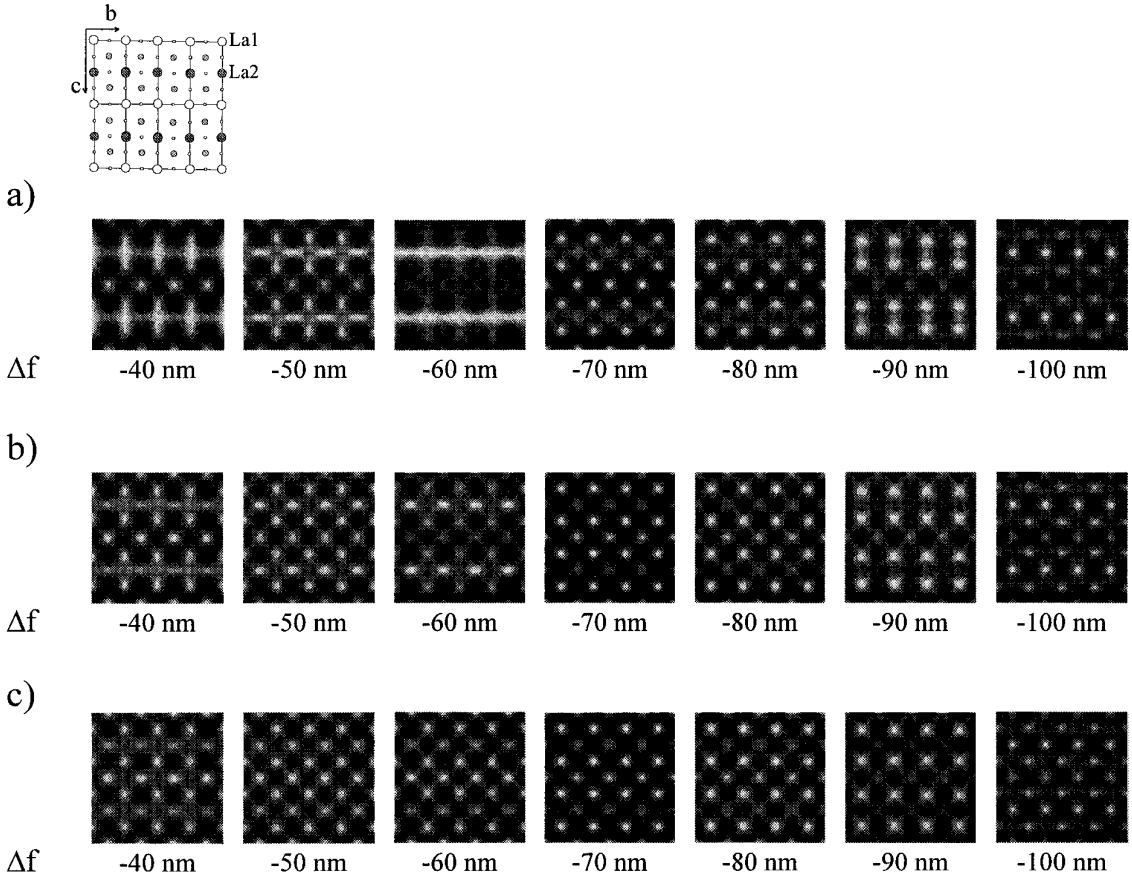

FIG. 14. Calculated ⟨100⟩ HREM images of a perfect crystal of the composition $x = 0.08$ with a specimen thickness close to 2.3 nm for different La1 (site 1*a*) and La2 (site 1*b*) occupancy rate: (a) site 1*a*, 100%; site 1*b*, 16.8%. (b) site 1*a*, 80%; site 1*b*, 36.8%. (c) site 1*a*, 60%; site 1*b*, 56.8%. The ⟨100⟩ projected crystal structure is given at the top of the simulated images: large open circles are relative to La1 atoms; large black circles are relative to La2 atoms; medium and small circles are, respectively, relative to Ti and O atoms.

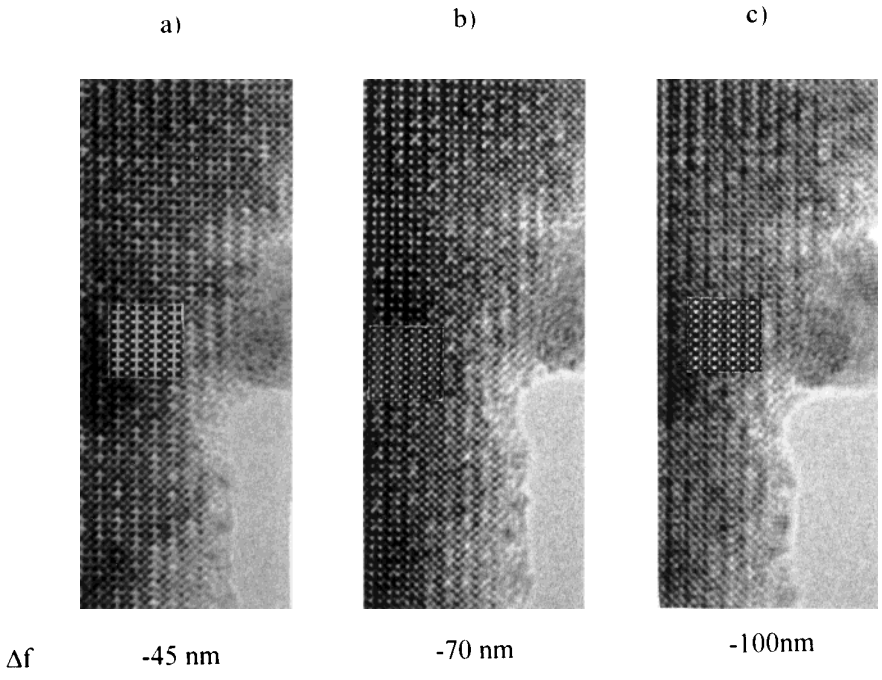

FIG. 15. Experimental and calculated ⟨100⟩ HREM images of a crystal of the composition $x = 0.08$ for three defocus values and a thickness close to 2.3 nm: (a) $\Delta f = -45$ nm, (b) $\Delta f = -70$ nm, and (c) $\Delta f = -100$ nm.

cus values close to that of Scherzer (−60 nm), a regular array of bright dots spaced by $a_p/\sqrt{2}$ along ⟨110⟩ direction. In our study, such contrast has never been observed, confirming thus the preferential occupation of one site by the La cations.

An example of ⟨100⟩ HREM images observed for three focus values is given Fig. 15 with the simulated images inserted (the La occupancy rates considered are, respectively, 91.2 and 25.6% for La1 and La2). The agreement between calculated and experimental images is rather good even if locally the real population of the two sites is not exactly that used to compute the simulations.

However, an important feature must be pointed out: an irregular contrast can be seen, more or less bright dots correlated only to the sites of La atoms (A or C rows) (Figs. 15 and 16). Such variations suggest an irregular distribution of the La atoms over their sites. Moreover, a careful examination of the HREM images reveals that these bright spots seem to be located only on one type of La sites (A or C rows). These remarks let us imagine that the occupation of one La site would be nearly constant (or show very small fluctuations) while the occupation of the other would be more irregular.

So, we attempted to simulate images showing ''anomalous'' contrast by using multislice simulations of supercells (wk3 program, slice thickness 0.387 nm, sampling 256 × 128). The best agreement is observed when the defect consists of a complete La vacancy on the site 1*b* (Fig. 17)

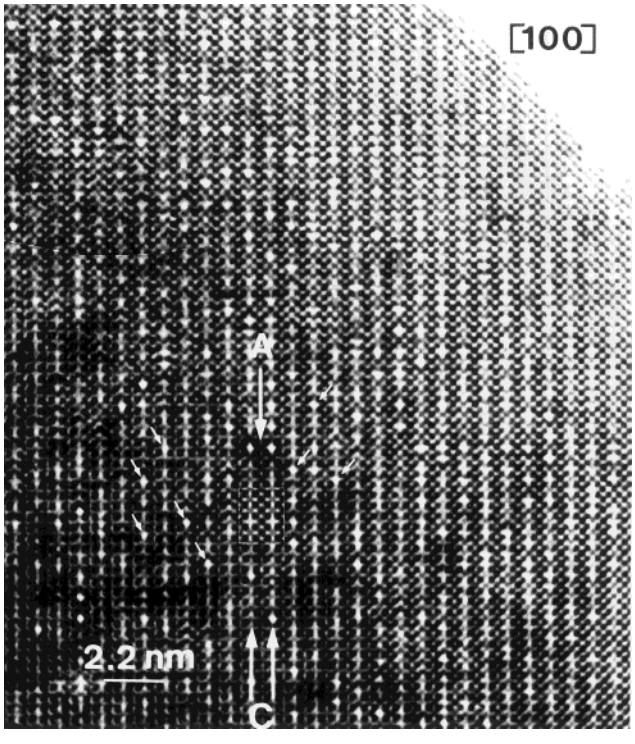

FIG. 16. ⟨100⟩ HREM image ($x = 0.08$) showing a lot of more bright dots ($\Delta f = -50$ nm, $t = 2.3$ nm) and the calculated image with zero cation occupancy on two La2 sites (same conditions as Fig. 17). White arrows show more pronounced bright dots located only on one type of rows (C).

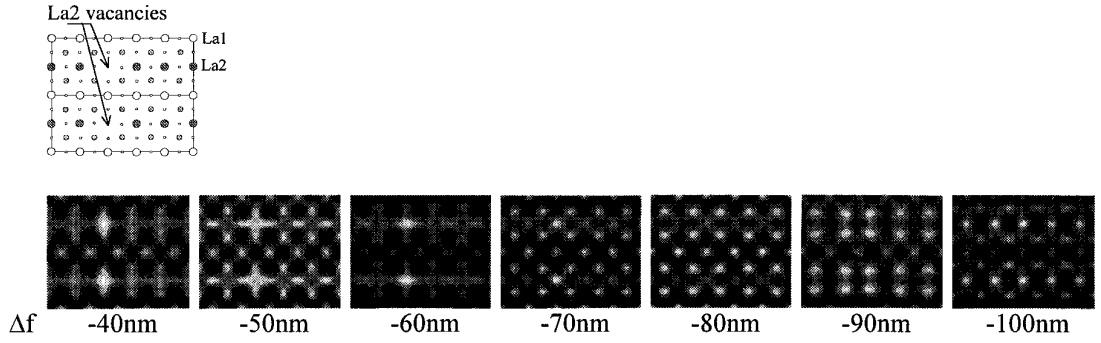

FIG. 17. Calculated ⟨100⟩ HREM images (t = 2.3 nm) of a crystal of the composition $x = 0.08$ with a complete La2 vacancy. The ⟨100⟩ projected crystal structure with the defect is shown at the top of the simulated images: large open circles are relative to La1 atoms; large black circles are relative to La2 atoms; medium and small circles are, respectively, relative to Ti and O atoms.

with the other sites occupancy rate close to that of $x = 0.08$ (respectively, 91.2 and 25.6% for La1 and La2). This means that at the position of the defect, for a 2.3 nm specimen thickness, all the six cationic positions are vacant (or occupied by Li cation). The ⟨100⟩ projected crystal structure with the defect is shown at the top of the simulated images. Note again that if the contrast of the calculated images is sensitive to the defect for several defocus values (−40 to −70 nm), it is nearly not affected for the others (−80 to −100 nm). In the first defocus range, the contrast reveals more pronounced bright dots at the La2 vacancy column. In the same time, the observed images of Figs. 15a and 15b show a contrast with a lot of brighter dots while that of Fig. 15c is more regular. Classically, it seems that the visibility of a local ordering of the La over its two respective sites is highly dependent of the focus and of the specimen thickness as mentioned by Cerva (21).

In order to compare the calculated and the observed HREM images, a higher magnification of the most sensitive images is given in Fig. 16 ($\Delta f = -50$ nm) with a simulated image inserted. This result suggests that the observed variations of the contrast may be correlated to a local arrangement of La atoms, vacancies, and Li atoms.

In the X-ray powder study, we have shown that further annealing of the sample $x = 0.11$ was without any effect on the shape of the superstructure diffraction lines and we have confirmed by HREM study that ⟨100⟩ images exhibit yet small domains and modulations of the contrast.

CONCLUSION

This study confirms the existence of a solid solution in the composition range $0.06 < x < 0.14$ in the series $La_{2/3-x}Li_{3x}\square_{1/3-2x}TiO_3$. X-ray powder diffraction and transmission electron microscopy experiments show that the symmetry is tetragonal ($P4/mmm$) with a unit cell (a_p, $2a_p$) deriving from that of the ABO_3 perovskite. The tetragonal distortion $c/2a$ vanishes strongly near $x = 0.08$. The value of this ratio $c/2a$ close to 1 allows the formation of multidomains 90° oriented in a preserved anionic network. The unequal distribution of the La over its two possible crystallographic sites involves the doubling of the a_p parameter along one direction. The width and the intensity of the surstructure lines (with $l = 2n + 1$) become broader and less intense as the Li content grows. These phenomena can be explained by the presence of antiphase domains which creates a disordered situation in the regular sequence …La1–La2–La1… along the c axis and by an unequal distribution of the La between the two possible sites. Moreover, the ⟨100⟩ HREM images show an irregular contrast which may be correlated to local La population fluctuations.

Further neutron diffraction studies are planned in order to specify the Li distribution.

REFERENCES

1. Y. Inaguma, C. Liquan, M. Itoh, T. Nakamura, T. Uchida, H. Ikuta, and M. Wakihara, *Solid State Com.* **86,** 689 (1993).
2. H. Kawai and J. Kuwano, *J. Electrochem. Soc.* **141**(7), L78 (1994).
3. J. Brous, I. Fankuchen, and E. Banks, *Acta Crystallogr.* **6**(1), 67 (1953).
4. P. V. Putil and V. S. Chincholkar, *Indian J. Chem. Sect. A* **16**(2), 95 (1978).
5. A. M. Varaprasad, A. L. S. Mohan, D. K. Chakrabarty, and A. B. Biswas, *J. Phys. C. Solid State Phys.* **12**(2), 465 (1979).
6. L. L. Kochergina, N. B. Khakhin, N. V. Porotnikov and I. Petrov, *Russ. J. Inorg. Chem.* **29**(4), 506 (1984).
7. A. Varez, F. Garcia-Alvarado, E. Moran, and M. A. Alario-Franco, *J. Solid State Chem.* **118,** 78 (1995).
8. J. Rodriguez Carjaval, "FULLPROF program: Rietveld Pattern Matching Analysis of Powder Patterns." ILL, Grenoble, 1990.
9. P. A. Stadelman, *Ultramicroscopy* **21,** 131 (1987).
10. A. D. Robertson, S. Garcia Martin, A. Coats, and A. R. West, *J. Mater. Chem.* **5**(9), 1405 (1995).
11. M. Abe and K. Uchino, *Mater. Res. Bull.* **9,** 147 (1974).
12. B. E. Warren, *in* "X-Ray Diffraction," p. 216. Addison-Wesley, Reading, MA, 1969.
13. R. D. Shannon, *Acta Crystallogr. Sect. A* **32,** 751 (1976).

14. V. K. Trunov, I. M. Averina, A. A. Evdokimov, and A. M. Frolov, *Sov. Phys. Crystallogr.* **26,** 1, 104 (1981).
15. R. J. White, R. L. Segall, J. C. Barry, and J. L. Hutchinson, *Acta Crystallogr. Sect. B* **41,** 93 (1985).
16. A. Vegas, M. Vallet-Regi, J. M. Gonzalez-Calbet, and M. A. Alario-Franco, *Acta Crystallogr. Sect. B* **42,** 167 (1986).
17. M. Labeau, I. E. Grey, J. C. Joubert, H. Vincent, and M. A. Alario-Franco, *Acta Crystallogr. Sect. A* **38,** 753 (1982).
18. J. M. Gonzalez-Calbet, M. Parras, M. Vallet-Regi, and J. C. Grenier, *J. Solid State Chem.* **92,** 110 (1991).
19. B. Raveau, C. Michel, M. Hervieu, and D. Groult, ''Crystal Chemistry of High-Tc Superconducting Copper Oxides,'' Springer Series in Materials Sciences 15, p. 189. Springer-Verlag, Berlin/New York.
20. M. A. Alario-Franco, I. E. Grey, J. C. Joubert, H. Vincent, and M. Labeau, *Acta Crystallogr. Sect. A* **38,** 177 (1982).
21. H. Cerva, *J. Solid State Chem.* **114,** 211 (1995).